Applied Ocean Research 170 (2026) 105028

Contents lists available at ScienceDirect

Applied Ocean Research

journal homepage: www.elsevier.com/locate/apor

Research paper

Computationally efficient spectral-domain wave-to-wire modeling of wave energy converters with geared rotary generators

Jian Tan [b], Ji Tao [c], Wei Tao [a,*], Chen Xi [b,d], George Lavidas [b], Hongda Shi [c]

[a] School of Mathematics and Computer Science, Wuhan Polytechnic University, 36, Huanhuzhonglu Road, Wuhan, 430048, China
[b] Faculty of Civil Engineering and Geosciences, Delft University of Technology, Stevinweg 1, 2628 CN, Delft, The Netherlands
[c] College of Engineering, Ocean University of China, 238, Songling Road, Qingdao, 266100, China
[d] Ocean College, Zhejiang University, Zhoushan, 316021, China

ARTICLE INFO

Keywords:
Spectral-domain modeling
Wave energy converter
Wave-to-wire analysis
Geared rotary generator

ABSTRACT

Wave-to-Wire (W2W) modeling simulates the whole operation process of wave energy converters (WECs), which plays a pivotal role in the systematic design and optimization of WECs. Existing W2W models are predominantly constructed based on time-domain (TD) analysis to coherently incorporate relevant nonlinearities. However, TD models require a high computational cost, which hinders the design iterations of WECs.

As a newly emerging alternative approach, spectral-domain (SD) modeling has demonstrated the applicability of describing the W2W process while efficiently covering nonlinear effects through statistical linearization. This study aims to develop an SD W2W modeling approach for WECs coupled with a gearbox and rotary generator. The application of the proposed model is exemplified in two case studies: (1) a point absorber with a rack-pinion system and a rotary generator; (2) a flap-type WEC with a revolving gearbox and a rotary generator. The simulation results obtained by the SD W2W model are compared against a higher-fidelity nonlinear TD W2W model to verify its accuracy across a variety of sea states. A good agreement between the two modeling approaches is observed, in which the maximum relative error is below 7 % with regard to the estimation of important system outputs. Meanwhile, the computational efficiency of the SD W2W model is thousands of times higher than the TD modeling approach.

1. Introduction

Ocean waves represent a vast source of clean, renewable energy. Over the past several decades, numerous wave energy converters (WECs) have been developed to harness this resource and generate electricity (Drew et al., 2009). Despite this progress, large-scale commercialization of WEC technology has not yet been achieved. Improving the competitiveness of WECs requires continuous advancements in design and performance. In this context, numerical modeling plays a critical role, offering an efficient and cost-effective alternative to experimental tests and sea trials, thereby accelerating WEC development.

Wave-to-Wire (W2W) modeling is a numerical approach used to assess the performance of WECs (Penalba and Ringwood, 2016). It characterizes the complete operation process, including wave-buoy hydrodynamics, energy transmission, and electricity generation (Folley, 2016). Through W2W models, the performance of WECs can be systematically analyzed. In recent years, various W2W models have been proposed and validated (Penalba and Ringwood, 2019; Penalba et al., 2017c,a), providing a more comprehensive representation of WECs compared to purely hydrodynamic models. For example, PTO parameters in WECs are typically tuned, based on hydrodynamic models, to maximize absorbed mechanical power by achieving the desired velocity or phase of the floater (Hals et al., 2010; Tan et al., 2020). However, studies have shown (Son and Yeung, 2017; Coe and Bacelli, 2023) that the conversion efficiency of electrical generators strongly depends on PTO parameters. Parameters optimal for mechanical power absorption are not necessarily optimal for electrical power production (Ringwood, 2025), a limitation that cannot be addressed by hydrodynamic models alone. Moreover, the efficiency of electrical generators in PTO systems is highly sensitive to WEC operating conditions (Blanco et al., 2025). For instance, Tan et al. (2022b, 2021) demonstrated that the efficiency of a linear generator in a point absorber could vary from around 70% in high-frequency waves to about 20% in low-frequency waves. Neglecting generator modeling may therefore lead to inaccurate estimates of actual power performance or annual energy production (AEP). Consequently, hydrodynamic models alone are insufficient for

* Corresponding author.
E-mail addresses: taowei@whpu.edu.cn, j.tan-2@tudelft.nl (W. Tao).

https://doi.org/10.1016/j.apor.2026.105028
Received 5 January 2026; Received in revised form 6 March 2026; Accepted 11 March 2026
Available online 26 March 2026

the design and optimization of WECs, highlighting the need for W2W models. In another recent study (Yi et al., 2026), a coupled wind–wave-to-wire modeling framework was proposed to simulate the entire operation process of a hybrid wind–wave energy system. That study clearly demonstrated the impact of nonlinear effects of multi-domain interactions on the overall system performance. In comparison, the coupled model in Yi et al. (2026) was established based on a time-domain (TD) approach, whereas the method proposed in the present study is developed within the spectral-domain (SD) framework. To the best knowledge of authors, existing W2W models are predominantly developed using TD approaches, aiming to capture nonlinear effects in power absorption, transmission, and conversion. However, as WEC technology remains in a pre-commercial stage, design and optimization inherently require a large number of iterations. Relying solely on TD W2W models renders this process computationally intensive and time-consuming. Thus, the development of more computationally efficient W2W models is expected to make a significant contribution to advancing WECs toward large-scale deployment.

SD modeling has gained attention as a computationally efficient alternative. Studies show it can be thousands of times faster than TD modeling while maintaining an error margin below 5% in operational conditions (Folley and Whittaker, 2010; Tan et al., 2022a). Unlike conventional Frequency-Domain (FD) approaches, SD modeling incorporates nonlinear effects through statistical linearization, assuming a Gaussian system response (De O. Falcão and Rodrigues, 2002). One of its earliest applications involved a flap-type WEC with quadratic damping and wave force decoupling, demonstrating strong agreement with TD results (Folley and Whittaker, 2010). Since then, SD modeling has been extended to account for nonlinear forces such as end-stop, mooring, viscous drag, Coulomb damping, and PTO constraints (Silva, 2019; da Silva et al., 2020; Silva et al., 2020; Spanos et al., 2018; Gunawardane et al., 2017; Tan et al., 2022a). Beyond the development of modeling methodologies, SD modeling has also been applied in previous studies to evaluate the performance of WECs, demonstrating a good balance between computational efficiency and accuracy (Bosma et al., 2012; Ermakov et al., 2024). Although SD modeling has proven effective for evaluating the hydrodynamics of WECs, its applicability to simulating the entire W2W process of WECs remains to be largely exploited. Only a few recent studies have investigated the potential of the SD modeling approach in modeling the entire W2W process. In Tan and Laguna (2023), a W2W model was developed based on the SD modeling approach for a single point-absorber WEC with a linear electric generator as the PTO system. In Tan et al. (2026), the SD W2W model was further extended to simulate WEC array formed by same point-absorber WECs with linear electric generator, in which the developed model was verified against a higher-fidelity TD model built in WEC-Sim. However, in the above-mentioned studies, the PTO system considered in the developed SD W2W models was limited to one specific type of PTO system, namely the linear generators. This severely hinders its applications to different types of WEC designs. Given the variability of PTO systems applied in WECs, W2W models are expected to possess wide applicability. In this sense, further research is needed to bridge this gap.

Mechanical-drive PTO systems, typically consisting of gearboxes coupled with rotary generators, have been widely considered a promising solution for power transmission in WECs. A key advantage of employing a gearbox is its ability to accelerate the motion of the WEC, since ocean waves generally occur at relatively low frequencies. The resulted increase in oscillation frequency is beneficial for improving generator efficiency (Polinder et al., 2006). Several studies have investigated the application of mechanical drive PTO systems in WECs. In Avalos et al. (2021) and Shadman et al. (2021), the influence of latching control on the power performance of a point absorber WEC with a gearbox and rotary generator was analyzed using a nonlinear TD W2W model. In Liang et al. (2017), a novel mechanical drive PTO system incorporating a mechanical motion rectifier was proposed, prototyped, and tested. This design converted bidirectional wave motion into unidirectional generator rotation by integrating two one-way bearings into a rack-and-pinion system. In Albert et al. (2017), an onshore flap-type WEC coupled with a gearbox was proposed, and its power performance in both regular and irregular seas was evaluated using a TD model. In Avalos et al. (2024), a point absorber WEC with a mechanical drive PTO was studied through a TD W2W model to provide a preliminary analysis of the relationships among gear ratio, device cost, and power performance. In Dang et al. (2019), the hydrodynamic performance and energy conversion efficiency of a rack-and-pinion-based WEC were experimentally investigated. The results showed that the PTO system achieved an overall efficiency of 80.4% and a capture width ratio as high as 41.6%. The above-mentioned studies collectively demonstrate the significant role of mechanical drive PTO systems in the energy transmission and conversion processes of WECs, which further underscores the necessity of developing a computationally-efficient SD model for WECs with mechanical PTO systems.

This work aims to develop an efficient SD approach to holistically simulate the W2W process of WECs with mechanical PTO systems, characterized by a gearbox coupled with a rotary permanent-magnet (PM) generator in this article. The proposed SD W2W model is expected to reveal the statistical properties of various performance indicators of the WEC system, such as dynamic motions, mechanical losses, electrical losses, and produced electrical power. Multiple significant nonlinear effects are incorporated in the SD W2W model via statistical linearization, including generator torque saturation, viscous drag force, friction losses and the current limit. This work presents, to the best of our knowledge, the first SD W2W modeling to incorporate a rotary PM generator with realistic nonlinearities in WECs. As such, it fills in the research gap of the SD W2W approach in modeling this particular class of PTO systems, which are adopted in WEC prototypes, such as Corpwer (Pennock et al., 2025). Two case studies are implemented to exemplify the application of the developed SD W2W modeling to WECs: (1) a point absorber with a rack-pinion system and a rotary PM generator; (2) a flap-type WEC with a gearbox and a rotary PM generator. A corresponding nonlinear TD W2W model is utilized as the verification reference, and a variety of sea states are considered in the verification.

The remainder of this paper is organized as follows. Section 2 presents the overall methodology, including the formulation of the TD W2W model and the development of the proposed SD W2W approach, together with the statistical linearization procedure. Section 3 introduces two representative case studies, namely a heaving point absorber and a flap-type WEC, and discusses the validation of the proposed model against the TD approach. Section 4 evaluates the computational efficiency of the proposed SD W2W model. Finally, Section 5 concludes the paper by summarizing the main findings and contributions.

2. Methodology

2.1. Workflow of WECs with a geared rotary generator

The workflow of WECs with a mechanical gearbox coupled with a rotary generator is illustrated in Fig. 1. The operation process of such types of WECs can be divided into four stages. First, the buoy of the WEC device is driven into oscillating motion by incoming waves, capturing their energy as kinetic energy. Depending on the type of WECs, the WEC buoy could move in different modes. Subsequently, the moving buoy drives the gearbox, which could convert the linear motion to rotation and/or further amplify the speed of rotation. For heaving WECs, rack/pinion systems can be adopted as the mechanical drive component to convert the linear motion to rotation of the pinion. For flap-type devices which perform rotary movement in the pitch mode, a revolving gearbox can be used to amplify the rotation speed of the oscillating flap. Followed by the stage of electricity generation, the output side of the gearbox drives the rotary generator to produce electricity. Meanwhile, the generator could provide a resistance force

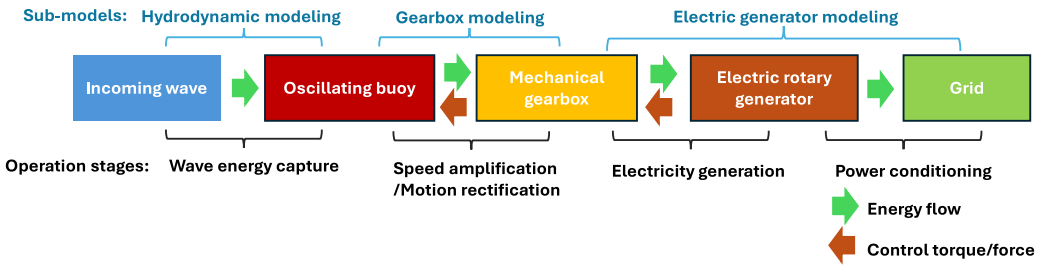

Fig. 1. Illustration of the W2W process and corresponding sub-models of WECs with mechanical PTO systems.

or torque acting on the WEC buoy via the gearbox for enhancing the power output. Finally, the electronic components are placed between the generator and the electric grid to improve the quality of the electric power.

As illustrated in Fig. 1, three sub-models are needed to comprehensively analyze the whole W2W process of WECs with mechanical PTO systems. The wave-buoy interaction is described by hydrodynamic modeling. Gearbox modeling is used to simulate the behavior of the gearbox and estimate the responses to various inputs. Electric generator modeling can be used to predict the generator's performance and electricity production, encompassing the processes from the gearbox output to the power grid. These models are integrated as a whole to be the so-called W2W modeling. In the next subsections, the W2W model based on TD analysis will first be presented. Subsequently, the development of the SD approach to simulate the W2W process will be detailed.

2.2. Time-domain W2W model

2.2.1. Representation of irregular waves

In this study, incoming waves are described following linear wave theory (Falnes, 2003). Based on the linear superposition, irregular waves can be represented by the summation of a range of regular wave components, as

$$\eta_{irr}(t) = \sum_{j=1}^{N} \zeta_a(\omega_j)\cos\left(k(\omega_j)x - \omega_j t + \varphi(\omega_j)\right) \tag{1}$$

where η_{irr} is the wave elevation of irregular waves, t is time, and $k(\omega_j)$, $\zeta_a(\omega_j)$, and $\varphi(\omega_j)$ represent the wave number, amplitude, and phase of the regular wave component at frequency ω_j. To represent irregular wave conditions, the wave spectrum is discretized into frequency bins of width $\Delta\omega$, and the wave amplitude at the frequency component ω_j is given as

$$\zeta_a(\omega_j) = \sqrt{2\,S(\omega_j)\Delta\omega} \tag{2}$$

where $S(\omega_j)$ is power spectral density corresponding to the frequency ω_j, and it can be derived based on given wave spectrum. JONSWAP spectrum is considered in this work, and the 200 discretized frequency components ranging from 0.1 to π. Although this work only applies the JONSWAP spectrum, the validity of the expression (1) holds for different types of wave spectra (Journée et al., 2015).

2.2.2. Hydrodynamic modeling

The floating buoy's interaction with incoming waves can be described via hydrodynamic modeling. The buoy's dynamics in the TD framework follow the Cummins equation (Cummins et al., 1962):

$$\left[M_{pto} + M + M_r(\infty)\right]a(t) = F_e(t) + F_{pto}(t) + F_{hs}(t) + F_{vis}(t) + \int_{-\infty}^{t} K_{rad}(t-\tau)u(\tau)d\tau \tag{3}$$

where:

M the buoy inertia;

M_{pto} overall inertia of the mechanical PTO system;

F_e the excitation force or moment;

F_{hs} the hydrostatic force or moment;

K_{rad} the impulse response function of radiation force;

$M_r(\infty)$ the added mass at the limit of infinite frequency F_{pto} the reaction force (rack/pinion system) or torque (revolving gearbox) exerted on the buoy;

u and a the buoy (angular) velocity and (angular) acceleration;

F_{vis} the viscous drag force or moment.

The terms $M_r(\infty)$ and K_{rad} are derived from hydrodynamic damping $R_r(\omega)$ and added mass $M_r(\omega)$. The excitation force in irregular waves can be expressed based on the derived excitation force coefficient $\hat{f}_e(\omega)$, as

$$F_e(t) = \sum_{j=1}^{N} \zeta_a(\omega_j)\hat{f}_e(\omega_j)\cos\left(\omega_j t + \varphi(\omega_j)\right) \tag{4}$$

These hydrodynamic coefficients, including $R_r(\omega)$, $M_r(\omega)$ and $\hat{f}_e(\omega)$, are computed in the frequency domain under the assumptions of linear potential flow theory using the Boundary Element Method (BEM) tool Nemoh (Penalba et al., 2017b). In the solver, the fluid is considered inviscid, incompressible, and irrotational, and the body is treated as rigid. The mean wetted surface of each WEC device, including both the point absorber and the flap-type WEC, is applied, and the linearized free-surface condition is assumed. It should be noted that viscous effects are not directly captured in the BEM computations. Instead, viscous drag is accounted for separately in the TD model through a quadratic damping term, as described below. To enhance computational efficiency, the convolution integral of the radiation force is approximated using a state-space representation following the method provided in Pérez and Fossen (2008).

Following Silva et al. (2020), the viscous drag force is approximated as a quadratic damping term:

$$F_{vis} = -\frac{1}{2}\rho C_D A_D |u(t)|u(t) \tag{5}$$

where ρ is water density, C_D the drag coefficient, and A_D the buoy's characteristic area perpendicular to motion.

The maximum torque that the rotary generator could produce is associated with a force or torque limit exerted on the buoy via the mechanical drive system, which is given as:

$$F_{pto}(t) = \begin{cases} -R_{pto}u(t), & if \quad |R_{pto}u(t)| \le F_{pto_{\mathrm{m}}} \\ \mathrm{sign}[-u(t)]F_{pto_{\mathrm{m}}}, & if \quad |R_{pto}u(t)| > F_{pto_m} \end{cases} \tag{6}$$

where F_{pto_m} denotes the maximum force/torque limit that the generator could provide via the mechanical PTO system to the buoy. The instantaneous absorbed power of the buoy can be expressed as

$$P_{ab}(t) = -F_{pto}(t)u(t) \tag{7}$$

2.2.3. Gearbox modeling

For heaving WECs, the gearbox, specifically the rack/pinion mechanism, converts the linear motion of the buoy to accelerated circular motion, driving the rotary generator. For rotating WECs, the revolving gearbox is normally applied to increase the rotation speed. In this work, the gearbox connections to the buoy and the generator are referred to as the input and output sides, respectively. The kinematic relation between the input and output sides of the gearbox can be expressed as

$$\omega_{out}(t) = r_{gear}u(t) \tag{8}$$

where ω_{out} is the angular velocity of the output side of the gearbox, r_{gear} is the gear ratio.

The shaft torque of the output side of the gearbox τ_{out} can be related to the force/torque on the buoy as

$$F_{pto}(t)u(t) - P_{gear} = -\tau_{out}(t)\omega_{out}(t) \tag{9}$$

where P_gear embodies the gearbox losses, considering friction losses, bearing losses, etc.

Referring to Polinder et al. (2006), the gearbox losses can be assumed to be proportional to rotation speed, which can be derived as

$$P_{gear}(t) = P_{gearm}\frac{|\omega_{ge}(t)|}{\omega_{gear,rated}} \tag{10}$$

where $\omega_{gear,rated}$ is the rated speed of the generator, P_{gearm} is the gearbox losses at the rated rotation speed, and it is assumed to be 1% of the rated power of the generator. Then, substituting (8) into (9), the torque on the output side of the gearbox is expressed as

$$\tau_{out}(t) = -\frac{F_{pto}(t)u(t) - P_{gear}}{r_{gear}u(t)} \tag{11}$$

As the output side of the gearbox is connected to the generator by a shaft, the generator torque is equal to the torque on the output gear, expressed as

$$\tau_{ge}(t) = \tau_{out}(t) \tag{12}$$

Similarly, there exists the relation:

$$\omega_{ge}(t) = \omega_{out}(t) \tag{13}$$

where ω_{ge} is the angular speed of the rotor of the rotary generator.

2.2.4. Generator modeling

In this study, an analytical electrical model is utilized to predict the performance of the electric generator, referring to Polinder et al. (2006). The primary function of the electric generator is to convert kinetic energy carried by the revolving shaft of the gearbox to usable electricity. The list of symbols of generator parameters is given in Table 1.

The relative motion between the rotor and stator of the machine induces a no-load voltage, which can be calculated as follows:

$$E_p(t) = \sqrt{2}\omega_{ge}(t)pr_r l_s N_s k_w|\hat{B}_{gm}| \tag{14}$$

where $\hat{B}_{gm}$ is the fundamental space harmonic of the magnetic flux density in the air gap resulting from the magnets (Polinder et al., 2004), p is the number of pole pairs, r_r is the radius of the rotor, l_s is the stack length, N_s is the number of conductors per slot, and k_w is the winding factor.

The iron losses are dependent on the generator frequency, which can be calculated as

$$P_{Fes} = P_{Fe0}\left[M_{Fest}\left(\frac{\hat{B}_{st}}{B_0}\right)^2 + M_{Fesy}\left(\frac{\hat{B}_{sy}}{B_0}\right)^2\right]\frac{f_e}{f_0} \tag{15}$$

where P_{Fe0} is the iron loss per unit mass at the frequency f_0 and flux density B_0; M_{Fest} and M_{Fesy} are the mass of the stator teeth and the stator yoke respectively; f_e is the electrical generator frequency which is dependent on the mechanical angular speed of the rotor, and $\hat{B}_{st}$ and $\hat{B}_{sy}$ embody the fundamental space harmonic of magnetic flux density in the stator teeth and yoke. $\hat{B}_{st}$ and $\hat{B}_{sy}$ can be calculated as

Table 1
Symbol list of the rotary PM generator.

Parameters	Symbol
Maximum average power	P_{rated}
Maximum torque	τ_{ge}
Rated rotation speed	ω_{rated}
Rotor radius	r_r
Rotor yoke height	h_{ry}
Rotor pole width	b_{rp}
Stack length	l_s
Air gap length	g
Stator slot width	b_{ss}
Stator yoke height	h_{sy}
Stator slot height	h_{ss}
Magnet pole width	b_p
Magnet pole pairs	p
Magnet thickness	l_m
Recoil permeability of the magnets	μ_{rm}
Remanent flux density of the magnets	B_{rm}
Iron loss per unit mass	P_{Fe0}
Copper resistivity	ρ_{Cu}
Copper fill factor	k_{sfil}
Number of conductors per slot	N_s
Number of slots per pole per phase	N_p

$$\hat{B}_{st} = \hat{B}_{gm}\frac{\chi_s}{b_t} \tag{16}$$

$$\hat{B}_{sy} = \hat{B}_{gm}\frac{\chi_p}{\pi h_{sy}} \tag{17}$$

where χ_s and χ_p are the slot pitch and pole pitch; b_t and h_{sy} are the tooth width and stator yoke height. The generator frequency is calculated as

$$f_e(t) = \frac{2\pi r_r|\omega_{ge}(t)|}{2\chi_p} \tag{18}$$

The power taken by the generator winding is obtained as the mechanical power absorbed minus the iron losses, expressed as

$$P_{wd} = \tau_{ge}(t)\omega_{ge}(t) - P_{Fes} \tag{19}$$

where P_{Fes} denotes the iron losses of the generator. In practice, these losses are insignificant compared to the absorbed power (Tan et al., 2022b). Furthermore, to improve system efficiency, the stator current I_s is typically controlled to be in phase with the no-load voltage E_p (Polinder et al., 2004). Accordingly, (19) can be rewritten as

$$P_{wd} \approx \tau_{ge}(t)\omega_{ge}(t) = mE_p(t)I_s(t) \tag{20}$$

where m represents the phase number of the electrical machine, and it is three in this case. It can be deduced from (20) that the linkage between the generator modeling and hydrodynamic modeling is built based on the balance between the power taken by the winding and the absorbed mechanical power. Substituting (14) to (20) gives the expression of the stator current:

$$I_s(t) = \frac{\tau_{ge}(t)}{m\sqrt{2}pr_r l_s N_s k_w|\hat{B}_{gm}|} \tag{21}$$

In electrical machines, there is an additional nonlinearity introduced by the electronic components, specifically the stator current limit I_{limit}. When the stator current approaches the limit, it reaches a saturation point and cannot increase further. The stator current limit is typically implemented to prevent the generator from overheating. It plays a significant role in determining the delivered grid power and overall system performance. Therefore, accounting for this effect is crucial in accurately evaluating the system's performance and ensuring its proper operation. As observed from Eq. (21), the stator current is directly linked to the PTO force. Consequently, the saturation of

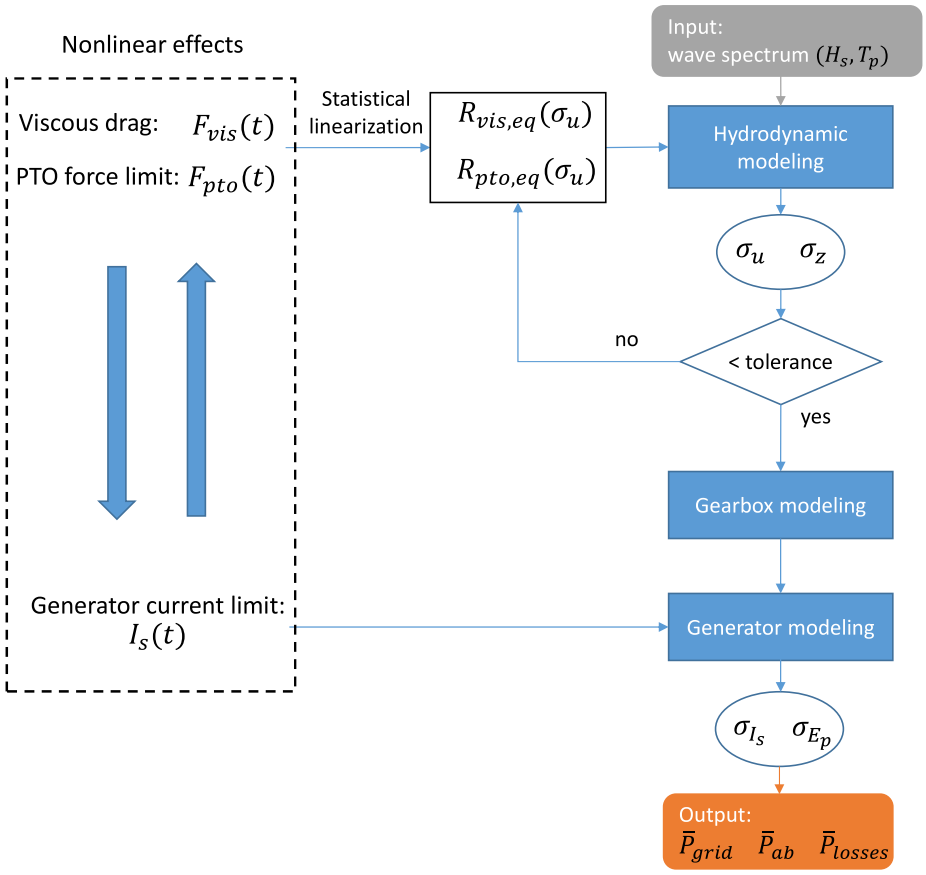

Fig. 2. Diagram of the proposed SD wave-to-wire modeling.

the PTO force is intrinsically influenced by the current limit. The impact of the current limit is equivalent to that of the PTO force limit in hydrodynamic modeling. Hence, there is no need to separately incorporate the stator current constraint in the generator modeling. For a given electrical machine, the force limit τ_{ge_m} is correlated with the stator current limit I_{limit} in the following manner:

$$\tau_{ge_m} = m\sqrt{2}pr_r l_s N_s k_w |\hat{B}_{gm}| I_{limit} \tag{22}$$

After the current I_s is derived, the copper losses can be calculated as

$$P_{copper}(t) = mI_s^2(t)R_t \tag{23}$$

where R_t is the stator phase resistance. For simplification, the converter losses P_{conv} are assumed to be only related to the generator side in this model, which can be expressed as

$$P_{conv} = \frac{P_{convm}}{31}\left[1 + 20\frac{|I_s(t)|}{I_{sm}} + 10\left(\frac{I_s(t)}{I_{sm}}\right)^2\right] \tag{24}$$

where P_{convm} is the power dissipation in the converter at the rated operating point, and it is assumed to be 3% of the converter's rated power (Polinder et al., 2006); I_{sm} is the rated current of the converter. In (24), the first term is a small constant part standing for the power dissipated in power supplies, gate drivers, control, and cooling system; the second term accounts for the major part that is proportional to the current, and this part is mainly related to the switching losses and conduction losses; the third term is proportional to the current squared, which corresponds to the conduction losses (Polinder et al., 2006).

As the gearbox losses and electrical losses have been derived, the usable electrical power delivered to the grid can be expressed as

$$P_{grid}(t) = P_{ab}(t) - P_{copper}(t) - P_{Fes}(t) - P_{gear}(t) - P_{conv}(t) \tag{25}$$

2.3. Spectral-domain approach

SD models are developed within the framework of FD modeling. In SD modeling, nonlinear effects are represented by equivalent linear coefficients in the equations of motion. These equivalent linear coefficients are determined through the process of statistical linearization. Previous studies in the literature have primarily focused on using SD models to predict the hydrodynamic responses of WECs (Silva et al., 2020; Silva, 2019; Folley and Whittaker, 2010, 2013). However, in this subsection, the SD modeling approach is extended to encompass the responses of electrical machines as well. The typical nonlinear effects arising from the electrical generator are linearized and incorporated into the SD model. By integrating these developments, the derived model allows for the calculation of the entire W2W responses using a purely SD approach. Fig. 2 provides a visual representation of the structure and solution process of the proposed SD W2W model.

2.3.1. Hydrodynamic modeling

As the wave input is considered as irregular waves, the excitation force at each frequency ω_j is expressed as

$$\hat{F}_e(\omega_j) = \zeta_a(\omega_j)e^{-i\phi_j}\hat{f}_e(\omega_j) \tag{26}$$

where $\zeta_a(\omega_j)$ is the wave amplitude of the wave spectrum at frequency ω_j, can be calculated referring to (2).

Based on superposition theory, the response caused by excitations of multiple frequencies can be described as the sum of the responses caused by each excitation source individually. In this sense, the dynamics of the WEC as a rigid body at each discretized frequency component can be described according to Newton's second law, as

$$\hat{F}_e(\omega_j) = [R_r(\omega_j) + R_{pto,eq} + R_{vis,eq}]\hat{u}(\omega_j) + i\omega_j\hat{u}(\omega_j)[M + M_r(\omega_j)] + i\hat{u}(\omega_j)(-\frac{K_{hs}}{\omega_j}) \tag{27}$$

where $R_{pto,eq}$ represent the equivalent damping coefficient of the PTO force or torque with saturation effect; $R_{vis,eq}$ denotes the equivalent damping coefficient of the viscous force. The contribution of nonlinear effects, including the force saturation and the viscous drag, to the dynamics of the floater is incorporated by these two equivalent linearized coefficients. The derivation of the equivalent coefficients will be detailed later in Appendix B.

Subsequently, the complex amplitude of velocity $\hat{u}$ could be obtained by solving (27) as

$$\hat{u}(\omega_j) = \frac{\hat{F}_e(\omega_j)}{R_r(\omega_j) + R_{pto,eq} + R_{vis,eq} + \mathrm{i}\omega_j[M + M_r(\omega_j)] - \mathrm{i}\frac{K_{hs}}{\omega_j}} \tag{28}$$

The standard deviation of the WEC velocity is therefore calculated as

$$\sigma_u = \sqrt{\sum_{j=1}^{N} \frac{1}{2}\left|\hat{u}(\omega_j)\right|^2} \tag{29}$$

The mean absorbed power can be further derived as

$$\begin{aligned}\overline{P}_{ab} &= \sum_{j=1}^{N} \frac{1}{2} R_{pto,eq}\left|\hat{u}(\omega_j)\right|^2 \\ &= R_{pto,eq}\sigma_u^2\end{aligned} \tag{30}$$

2.3.2. Gearbox modeling

As given in (11), the delivered torque on the output side of the gearbox is related to both the buoy dynamics and the gearbox losses. However, as the gearbox losses are mostly considered negligible compared to the absorbed power of WECs (Penalba and Ringwood, 2016), the output torque of the gearbox in the SD approach can be approximated as

$$\tau_{ge}(\omega) \approx -\frac{\hat{F}_{pto}(\omega)}{r_{gear}} \tag{31}$$

The kinetic relation of the gearbox can be presented as

$$\begin{aligned}\hat{\omega}_{ge}(\omega_j) &= \hat{\omega}_{out}(\omega_j) \\ &= r_{gear}\hat{u}(\omega_j)\end{aligned} \tag{32}$$

In the SD approach, the mean friction losses of the gearbox can be derived, referring to (10), as

$$\begin{aligned}\overline{P}_{gear} &= \langle P_{gearm}\frac{|\hat{\omega}_{ge}(\omega_j)|}{\omega_{rated}}\rangle \\ &= \frac{P_{gearm}}{\omega_{rated}}\langle|\hat{\omega}_{ge}(\omega_j)|\rangle\end{aligned} \tag{33}$$

As ω_{ge} is assumed to be a Gaussian variable, the expected value of its absolute value is expressed as

$$\langle|\hat{\omega}_{ge}(\omega_j)|\rangle = \sqrt{\frac{2}{\pi}}\sigma_{\omega_{ge}} \tag{34}$$

It should be noted that the Gaussian assumption of ω_{ge} is valid under the conditions of linear wave theory and direct mechanical coupling between the floater and the generator, with no motion rectification mechanism equipped in the PTO drivetrain.

2.3.3. Generator modeling

As presented above, the hydrodynamic and gearbox models built upon the SD approach can be used to describe the transmission flow of the mechanical power, while a generator model is needed to analyze the power conversion undertaken by electric generators. Assuming a random phase distribution of wave inputs to the WEC system, it is feasible to represent the generator responses within the framework of the SD modeling.

Based on (14), the complex amplitude of the no-load voltage in each frequency component is expressed as

$$\hat{E}_p(\omega_j) = \sqrt{2}\hat{u}(\omega_j)pr_r l_s N_s k_w|\hat{B}_{gm}| \tag{35}$$

where

$\hat{B}_{gm}$ the fundamental space harmonic of the magnetic flux density;
p the number of pole pairs;
r_r the radius of the rotor;
l_s the stack length;
N_s the number of conductors per slot;
k_w the winding factor. The parameters for different types of WECs considered in this study are specified in Table A.5 and A.6.

The power taken by the generator winding, namely P_{wd}, at each frequency component is calculated as

$$\begin{aligned}P_{wd}(\omega_j) &= \frac{1}{2}\mathrm{Re}\{\hat{F}_{pto}(\omega_j)\hat{u}^*(\omega_j)\} \\ &= \frac{1}{2}|\hat{F}_{pto}(\omega_j)||\hat{u}(\omega_j)| \\ &= \frac{1}{2}R_{pto,eq}|\hat{u}(\omega_j)|^2\end{aligned} \tag{36}$$

Thus, the magnitude of the complex amplitude of the stator current at each frequency component can be calculated as

$$|\hat{I}_s(\omega_j)| = \frac{R_{pto,eq}|\hat{u}(\omega_j)|^2}{m|\hat{E}_p(\omega_j)|} \tag{37}$$

As the effect of the PTO force or torque limit has been incorporated by the equivalent linear coefficient $R_{pto,eq}$, the current limit is therefore taking effect correspondingly. Then, the standard deviation of the stator current is derived as

$$\sigma_{I_s} = \sqrt{\frac{1}{2}\sum_{j=1}^{N}|I_s(\omega_j)|^2} \tag{38}$$

The copper losses of the generator can be calculated as follows:

$$\begin{aligned}\overline{P}_{copper} &= \langle mI_s^2 R_t\rangle \\ &= mR_t\sigma_{I_s}^2\end{aligned} \tag{39}$$

This enables the prediction of the converter losses, expressed as

$$\begin{aligned}\overline{P}_{conv} = \frac{1}{31}P_{convm} + \frac{20}{31I_{sm}}P_{convm}\langle|I_s|\rangle + \\ \frac{10}{31I_{sm}^2}P_{convm}\langle I_s^2\rangle\end{aligned} \tag{40}$$

Assuming that the variable I_s follows the Gaussian distribution, it gives

$$\langle|I_s|\rangle = \sqrt{\frac{2}{\pi}}\sigma_{I_s} \tag{41}$$

The iron losses are calculated as

$$\overline{P}_{Fes} = P_{Fe0}\left[m_{Fest}\left(\frac{\hat{B}_{st}}{B_0}\right)^2 + m_{Fesy}\left(\frac{\hat{B}_{sy}}{B_0}\right)^2\right]\frac{\langle f_e\rangle}{f_0} \tag{42}$$

where $\langle f_e\rangle$ can be related to the standard deviation of the absolute value of the buoy velocity, and assuming the Gaussian assumption of the response gives

$$\begin{aligned}\langle f_e\rangle &= \langle\frac{2\pi}{2\chi_p}|\hat{\omega}_{ge}|r_r\rangle \\ &= \frac{\pi}{\chi_p}\langle|\hat{u}|\rangle r_{gear}r_r \\ &= \frac{\pi}{\chi_p}\sqrt{\frac{2}{\pi}}\sigma_u r_{gear}r_r\end{aligned} \tag{43}$$

Therefore, the mean grid power can be derived as

$$\overline{P}_{grid} = \overline{P}_{ab} - \overline{P}_{copper} - \overline{P}_{Fes} - \overline{P}_{gear} - \overline{P}_{conv} \tag{44}$$

3. Case studies

3.1. Case study 1: Point absorber with a rack-pinion system and a rotary generator

3.1.1. Concept description

The studied WEC concept is illustrated in Fig. 3, and the main parameters are given in Table 2. The WEC system contains two main

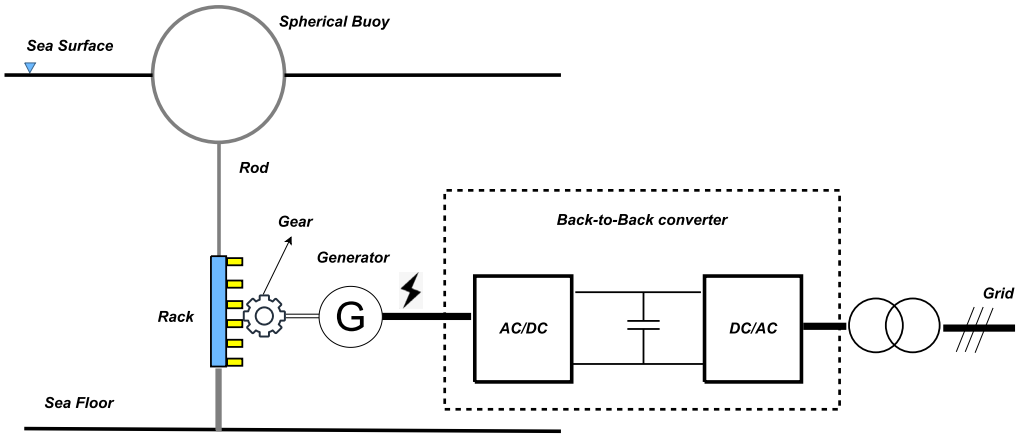

Fig. 3. Schematic of the spherical heaving point absorber with a bottom-founded geared rotary PM generator (Tan et al., 2022b).

Table 2
Simulation parameters of case study 1.

Parameters	Quantities
Sphere radius	2.5 m
Sphere draft	2.5 m
Sphere mass: M	33 543 kg
overall PTO inertia: M_{pto}	200 kg
PTO damping: B_{pto}	100 kN s/m
Water depth	100 m
Water density: ρ	1025 kg/m^3
Gear ratio: r_{gear}	4

components: the floating captor and the PTO system. The floating captor is represented by a spherical buoy with a diameter of 5 m. Designed to partially submerge in calm water, the buoy has a density half that of water. Incoming waves trigger vertical oscillations, converting wave energy into mechanical power. Comparatively, the PTO system converts the mechanical motion of the floater to usable electrical power. The floating buoy is connected to the PTO system by a rod. The PTO system consists of a rack-pinion system, a rotary PM generator and a back-to-back voltage converter. The linear movement of the floating buoy is converted to circular motion by the rack and pinion system, which is then used to drive the rotary PM generator. The electrical inverter, connected to the output side of the machine, is implemented as a three-phase back-to-back converter (Polinder et al., 2004). The design of this generator is inspired by the electrical machine used in the work (Polinder et al., 2006) for a generator concept for wind turbines. However, it has been scaled down from the original reference machine to match the dimensions of the buoy employed in this study. The scaling process follows the principle of maintaining an identical force density per unit area of the active surface of the electrical machines. More detailed information regarding the scaling of electrical machines can be found in Tan et al. (2021). The machine parameters considered in this study are outlined in Table A.5.

3.1.2. Simulation results

This section presents the simulation results of the SD W2W model, validated against the TD model across various wave conditions. Fig. 4 compares the standard deviation of the buoy velocity, the stator current, and the no-load voltage, along with the relative errors of the SD model. The maximum errors are 5% for the stator current, 6% for the no-load voltage, and 3% for the buoy velocity, increasing slightly with higher wave heights due to intensified nonlinear effects. The results suggest the effectiveness of the proposed model in estimating the dynamic and electrical responses of the WEC system.

The W2W modeling framework facilitates a thorough assessment of power conversion efficiency across the entire system operation. To comprehensively demonstrate the capability of the established SD W2W model, the losses at each power transmission stage, the electrical power supplied to the grid, and the corresponding conversion efficiencies are evaluated against those evaluated by the TD model. Power conversion efficiency, measured as the ratio of electrical power delivered to the grid to the mechanical power absorbed by the floater, is a key performance metric in the performance assessment of WECs. Fig. 5 presents the power, losses and the power conversion efficiencies estimated by the SD W2W and TD W2W models. Additionally, the relative errors of the proposed SD model to the TD W2W model are identified in Fig. 6, in which their estimations of the grid power are taken into account. It is visible that the proposed SD model closely aligns with the TD model in estimating the results in different operation stages, maintaining relative errors below 6% even at a significant wave height of 4 m and under 2% for milder sea states ($H_s < 2.5$ m). These observations imply that the SD model's reliability in estimating power conversion efficiency. As a consequence, the proposed SD W2W model can be applied as an effective alternative to the TD W2W models for analyzing the systematic performance or performing design optimizations of WECs.

3.2. Case study 2: Flap-type WEC with a revolving gearbox and a rotary PM generator

3.2.1. Concept description

In the second case study, the proposed SD W2W model is utilized to simulate the flap-type WEC. As illustrated in Fig. 7, the flap of the WEC is excited by incoming waves to rotate about the hinge bottom-founded at the seabed, and the mechanical PTO system is placed in the chamber of the hinge. The mass of the flap is assumed to be evenly distributed in the volume, and the mass density is considered 250 kg/m^3. In the mechanical PTO system, the rotating flap drives the PM rotary generator through a revolving gearbox in which the rotation speed is increased to improve the generator efficiency. A three-phase back-to-back voltage converter is used to regulate the generated electricity and then transfer it to the grid as usable electricity. Some important simulation parameters of the flap-type WEC are given in Table 3, while more detailed design parameters of the electrical generator can be found in Table A.6.

3.2.2. Simulation results

The simulation results of the W2W process of the flap-type WEC are presented in Figs. 8 and 9. Fig. 8 depicts the estimation of the standard deviation of the angular velocity of the flap, the no-load voltage, and the stator current across different peak periods and significant wave heights. It is visible that the proposed SD W2W model presents highly comparable results with those obtained by the nonlinear TD W2W model, even at high wave conditions. For instance, at the significant

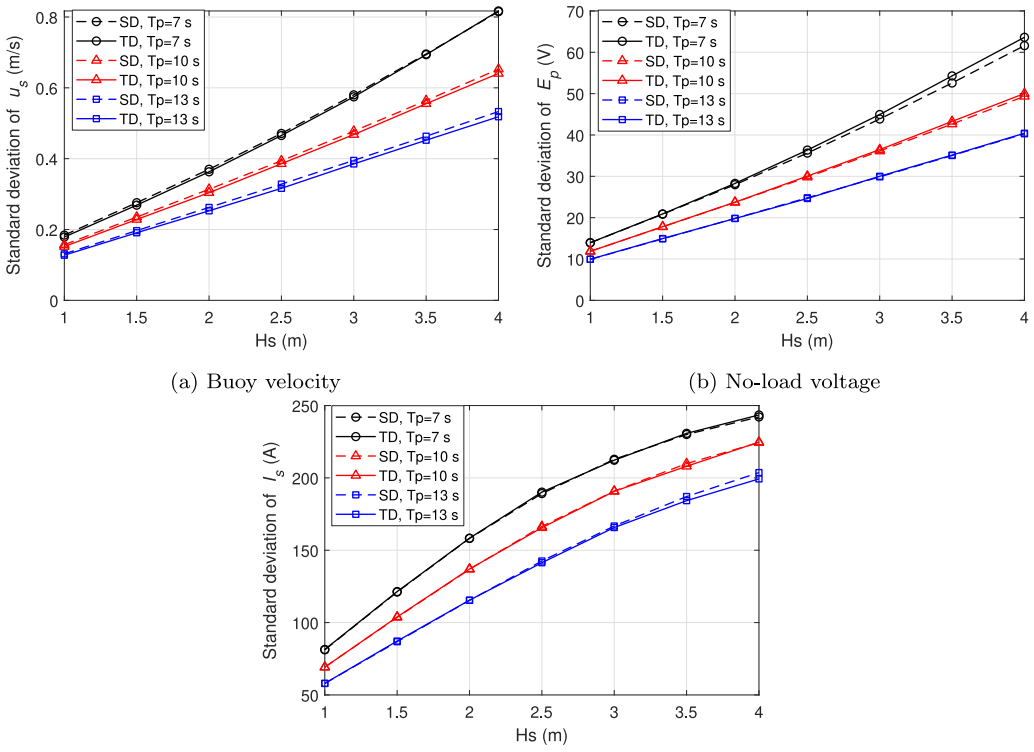

(a) Buoy velocity (b) No-load voltage

(c) Stator current

Fig. 4. The standard deviation of the responses of the point absorber WEC in different wave states of the SD W2W model to the TD W2W model. (B_{pto} = 100 kN s/m)

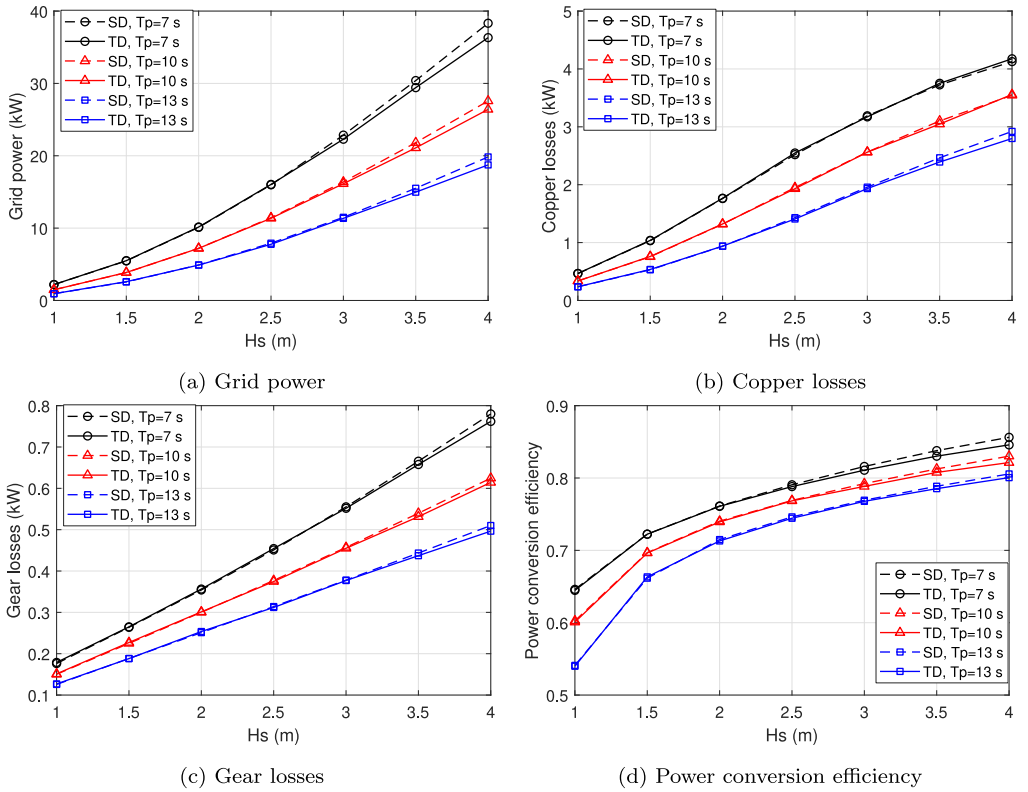

(a) Grid power (b) Copper losses

(c) Gear losses (d) Power conversion efficiency

Fig. 5. Grid power, copper losses and power conversion efficiency of the point absorber WEC in different wave states.

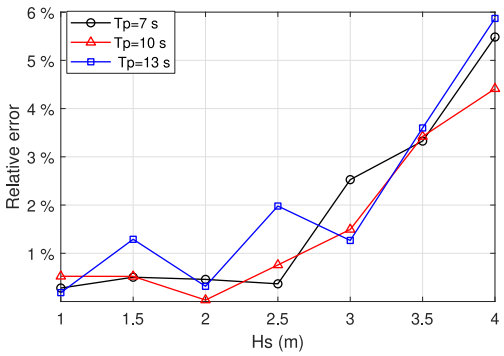

Fig. 6. The relative errors of the established SD W2W model to the TD W2W model with regard to the estimation of the grid power of the point absorber WEC.

Table 3
Simulation parameters of case study 2.

Parameters	Quantities
Flap width:	2 m
Flap length:	12 m
Flap height:	10 m
Flap draft:	9 m
Water depth:	11 m
Moment of inertia of flap: M	2 785 000 kg m^2
Overall mechanical PTO inertia: M_{pto}	15 000 kg m^2
PTO damping: B_{pto}	10 000 kN s/rad
Hydrostatic stiffness:	6824 kN m/rad
Drag coefficient:	2
Water density: ρ	1025 kg/m^3
Gear ratio: r_{gear}	3

wave height of 4 m and peak period of 13 s, the standard deviation of the stator current estimated by the SD W2W model is around 310 A, while it is approximately 330 A for the nonlinear TD W2W model. The relative error between the two models appears to be 6.1% in this high wave condition. The calculated grid power, conversion losses, and conversion efficiency of the WEC are presented in Fig. 9. It is seen that the SD W2W model shows a good agreement with the nonlinear TD W2W model at different sea states. The relative error of the SD model to the TD model on the estimation of the grid power is given in Fig. 10, considering different sea states. The maximum relative error is no more than 6% in this case.

4. Computational efficiency

The main advantage of the SD approach is its ability to capture nonlinear effects with high computational efficiency. Table 4 compares the simulation times of the two modeling approaches, with all runs performed on the same machine, equipped with an Intel i7 processor (2.80 Hz), under identical conditions. For the TD model, the presented computational time corresponds to 30 runs of simulation with different sets of random phase angles of superpositions for incoming waves. This is intended to obtain averaged results and suppress random errors (Folley, 2016). As shown in Table 4, the proposed SD W2W model reduces computational effort by nearly 2000 times compared to the TD W2W approach. This efficiency makes it particularly well-suited for tasks that demand extensive simulations, such as WEC array optimization.

5. Discussion

The main limitations of this study lies on three aspects. First, although the prediction results of the proposed SD W2W model are in good agreement with those of the nonlinear TD W2W model, the relative error exhibits an increasing trend with the significant wave

Table 4
Comparison of computational time of W2W modeling approaches for one simulation case. Simulation conditions are $T_p = 9$ s and $H_s = 4$ m.

Array configurations	Numerical models	Computational time
Case 1	SD	6.2×10^{-2} s
	TD	151.7 s (30-runs)
Case 2	SD	7.9×10^{-2} s
	TD	163.2 s (30-runs)

height. This behavior is primarily attributed to the Gaussian process assumption adopted in the statistical linearization procedure, which constitutes the main source of discrepancy. As the nonlinear effects in the system become stronger, the validity of the Gaussian assumption gradually deteriorates. Under powerful sea states, the intensified nonlinearities inevitably reduce the accuracy of the proposed SD model, as discussed in Folley and Whittaker (2010) and Tan and Lavidas (2024).

Secondly, the equation of motion of the SD W2W model is formulated in the frequency domain with statistically linearized correction terms which derived based on random phases. Therefore, it is restricted to providing stationary statistical results, such as mean values, variances, and standard deviations of relevant variables. It does not generate explicit time-dependent results of system responses. Consequently, it cannot directly used to analyze the detailed transient behavior, such as peak responses or loads in short time durations.

Thirdly, the proposed SD W2W model is inherently limited to linear wave theory. The hydrodynamic coefficients employed in the SD W2W model are derived from linear potential flow theory, which assumes small wave steepness and small body motions. Under mild to moderate sea states, this assumption remains rather valid. However, in more severe conditions, nonlinear hydrodynamic effects, such as nonlinear Froude–Krylov forces and wave slamming, may become significant. Since these effects are not considered in the SD modeling, the applicability of the SD model is constrained to operating regimes where wave and motion nonlinearities remain within a moderate range.

6. Conclusion

A spectral-domain (SD) modeling approach is developed in this work to simulate the entire wave-to-wire (W2W) process of WECs with geared rotary generators. Nonlinear effects throughout the process, including viscous drag force, PTO force/torque limit, gear losses, generator current limit and electrical losses, are efficiently incorporated in the proposed SD W2W model via statistical linearization. The proposed SD W2W model is applied to two typical case studies: (1) a heaving point absorber with a rack-pinion system coupled with a rotary PM generator; (2) a flap-type device with a gearbox coupled with a rotary PM generator. The simulation results are verified against a nonlinear time-domain (TD) W2W model. Conclusions are drawn below:

The SD W2W model demonstrates good accuracy in estimating the WEC's responses in different operation stages. In the first case study, the relative errors of the SD approach to the TD approach are no more than 5% for the standard deviation of the stator current, 6% for the standard deviation of the no-load voltage, and 6% for the estimated mean grid power estimation. As for the second case study, the maximum relative error is lower than 6.1% for the estimated standard deviation of the dynamic or electrical responses, and it is 6% for the estimation of the mean grid power.

The high computational efficiency of the proposed SD model stands out as a strong merit of this approach. In both case studies, the proposed SD W2W model is approximately 2000 times faster than the conventional TD model, making it highly aligned with the demand for computationally efficient simulation tools in early-stage and large-scale WEC design and optimization of WECs.

Beyond the quantitative validation results, this study contributes to

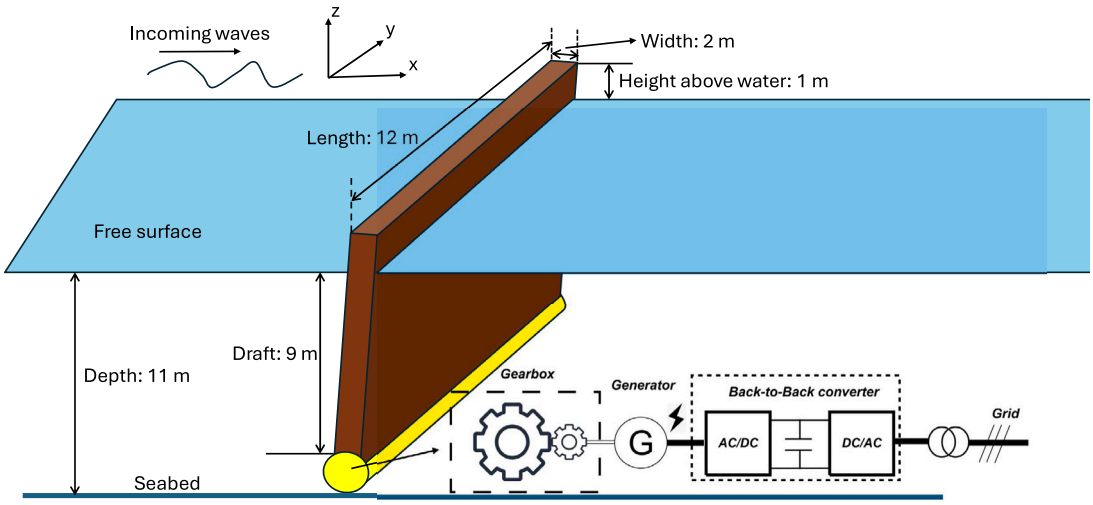

Fig. 7. Schematic of the flap-type WEC with a bottom-founded gearbox and a rotary PM generator.

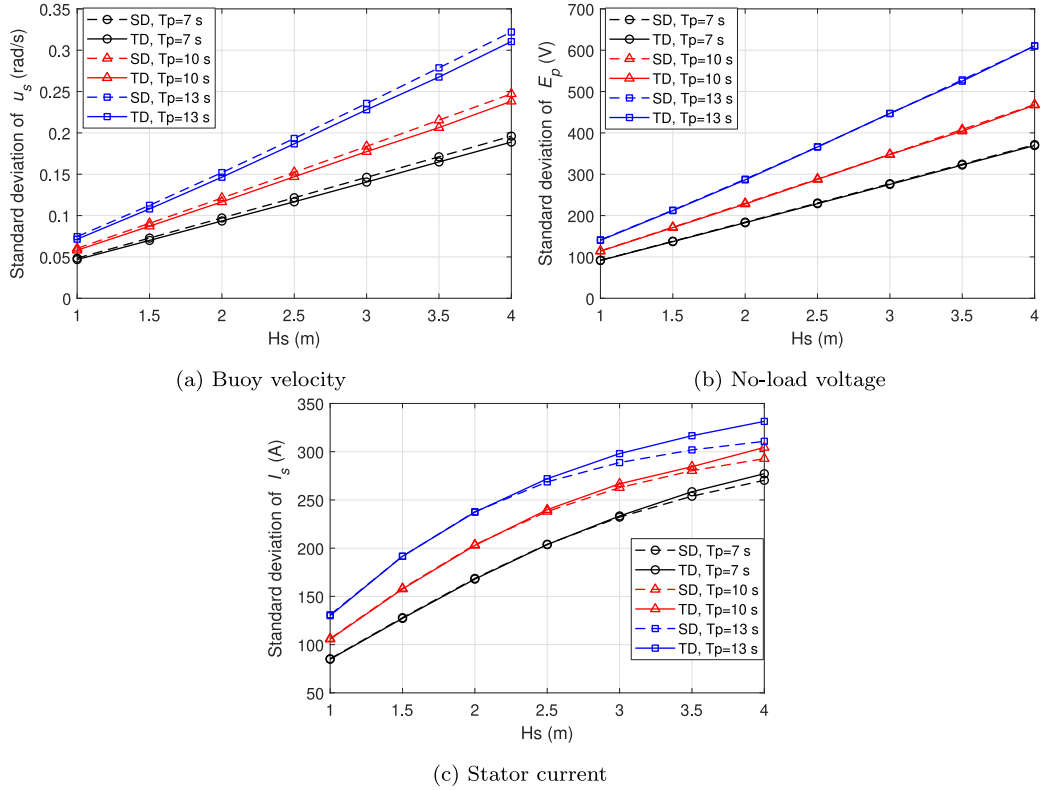

(a) Buoy velocity

(b) No-load voltage

(c) Stator current

Fig. 8. The standard deviation of the responses of the flap-type WEC in different wave states.

the theoretical advancement of marine renewable by extending the SD modeling framework from purely hydrodynamic response analysis to a fully coupled W2W representation for WECs equipped with mechanical PTO systems. In particular, the key nonlinear effects arising throughout the multi-stage energy conversion process are derived as statistically linearized equivalent coefficients, enabling their systematic incorporation into the SD framework while maintaining satisfactory accuracy. This methodology provides a novel perspective for unifying hydrodynamic modeling with power transmission and power conversion modeling in WEC systems.

From a practical perspective, the proposed SD W2W model serves as a computationally efficient tool capable of substantially accelerating design iterations, parameter optimization, and techno-economic assessments of WECs with mechanical-drive PTO systems. Its ability to rapidly evaluate power production, conversion efficiency, and loss distribution across a broad range of sea states makes it particularly well suited for large-scale parametric analyses, control parameters tuning, and preliminary sizing of gearboxes and generator components. Furthermore, the significant reduction in computational cost enhances its applicability to WEC array optimization and long-term energy yield assessments, which typically require extensive time-duration simulations. By enabling fast yet sufficiently accurate performance predictions, the developed model supports informed decision-making during early-stage technology development and contributes to reducing overall development costs associated with wave energy commercialization.

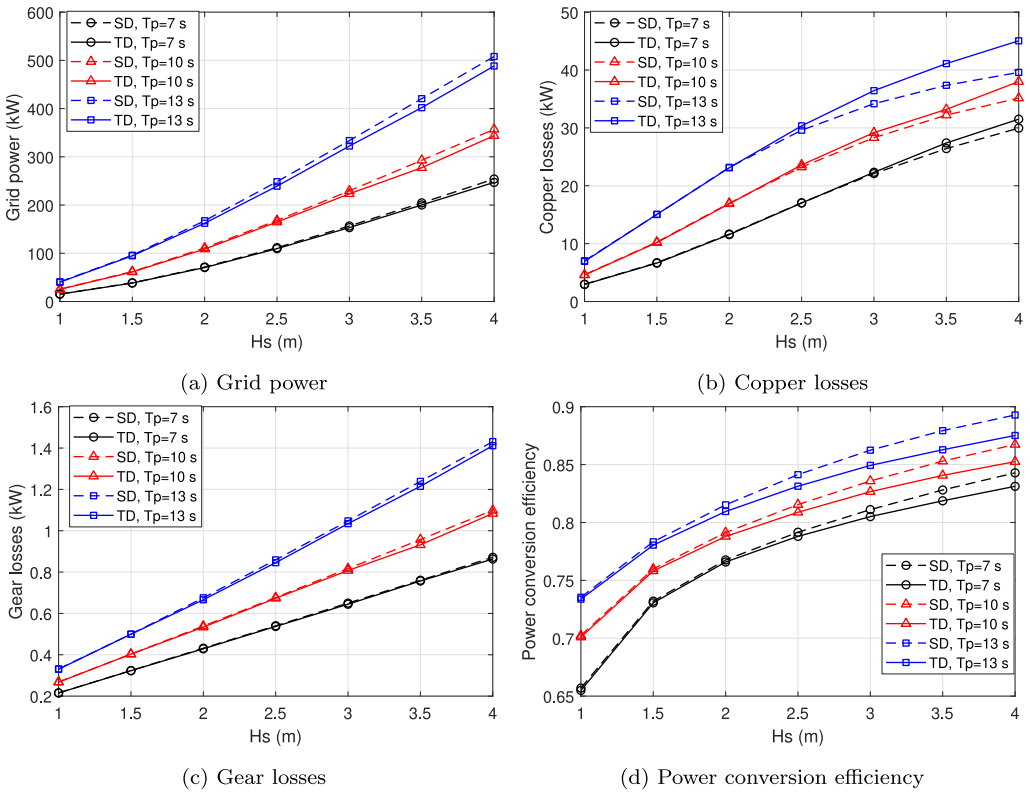

Fig. 9. Grid power, copper losses and power conversion efficiency of the flap-type WEC in different wave states.

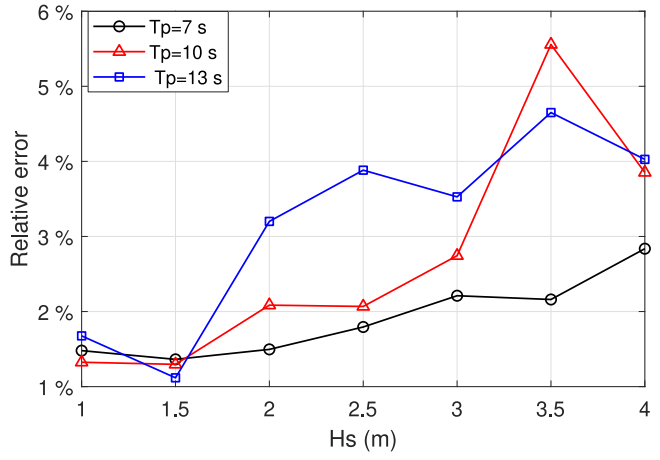

Fig. 10. The relative errors of the established SD W2W model to the TD W2W model with regard to the estimation of the grid power of the flap-type WEC.

CRediT authorship contribution statement

Jian Tan: Writing – original draft, Visualization, Validation, Supervision, Software, Resources, Project administration, Methodology, Investigation, Formal analysis, Data curation, Conceptualization. **Ji Tao:** Writing – review & editing, Visualization, Validation, Supervision, Software, Resources, Project administration, Methodology, Investigation, Formal analysis, Data curation, Conceptualization. **Wei Tao:** Writing – review & editing, Visualization, Validation, Supervision, Resources, Project administration, Methodology, Investigation, Formal analysis, Data curation, Conceptualization. **Chen Xi:** Writing – review & editing, Visualization, Validation, Software, Methodology, Formal analysis, Data curation. **George Lavidas:** Writing – review & editing, Visualization, Supervision, Software, Resources, Project administration, Investigation, Funding acquisition, Formal analysis, Data curation, Conceptualization. **Hongda Shi:** Writing – review & editing, Visualization, Validation, Supervision, Software, Resources, Project administration, Methodology, Investigation, Formal analysis, Data curation, Conceptualization.

Declaration of competing interest

The authors declare that they have no known competing financial interests or personal relationships that could have appeared to influence the work reported in this paper.

Acknowledgments

This research was also funded by the Young Talents Project of the Science Research Program of Hubei Provincial Department of Education through grant No. 2023Q20231606, the Dutch Research Council (Nederlandse Organisatie voor Wetenschappelijk Onderzoek-NWO) with Project No. EP.1602.22.001 and the CETPartnership, the Clean Energy Transition Partnership under the 2022 CETPartnership joint call for research proposals, co-funded by the European Commission (GAN° 101069750) Project No. CETP-2022-00127.

Appendix A. Design parameters of utilized rotary generators

The electrical machine parameters considered in case study 1 and case study 2 are outlined in Tables A.5 and A.6, respectively.

Appendix B. Statistical linearization

The primary objective of statistical linearization is to ensure that the expected value of the dissipated power matches that of the equivalent linear term. Statistical linearization has been applied in a series of recent studies (Tan et al., 2025a,b, 2022a; Folley and Whittaker, 2010)

Table A.5
Specification of the sized generator for case study 1.

Parameters	Symbol	Quantities
Maximum average power	P_{rated}	157 kW
Maximum torque	τ_{ge}	20 kN m
Rated rotation speed	–	75 rpm
Rotor radius	r_r	0.41 m
Rotor yoke height	h_{ry}	40 mm
Rotor pole width	b_{rp}	82 mm
Stack length	l_s	0.4 m
Air gap length	g	3.6 mm
Stator slot width	b_{ss}	15 m
Stator yoke height	h_{sy}	40 mm
Stator slot height	h_{ss}	80 mm
Magnet pole width	b_p	79 mm
Magnet pole pairs	p	13
Magnet thickness	l_m	15 mm
Recoil permeability of the magnets	μ_{rm}	1.1
Remanent flux density of the magnets	B_{rm}	1.1 T at 85 °C
Iron loss per unit mass	P_{Fe0}	4.9 W/kg at 50 Hz and 1.5 T
Copper resistivity	ρ_{Cu}	0.0252 μΩm at 120 °C
Copper fill factor	k_{sfil}	0.6
Number of conductors per slot	N_s	6
Number of slots per pole per phase	N_p	1

Table A.6
Specification of the sized generator for case study 2.

Parameters	Symbol	Quantities
Maximum average power	P_{rated}	1000 kW
Maximum torque	τ_{ge}	700 kN m
Rated rotation speed	–	50 rpm
Rotor radius	r_r	1.8 m
Rotor yoke height	h_{ry}	40 mm
Rotor pole width	b_{rp}	82 mm
Stack length	l_s	1 m
Air gap length	g	3.6 mm
Stator slot width	b_{ss}	15 m
Stator yoke height	h_{sy}	40 mm
Stator slot height	h_{ss}	80 mm
Magnet pole width	b_p	79 mm
Magnet pole pairs	p	46
Magnet thickness	l_m	15 mm
Recoil permeability of the magnets	μ_{rm}	1.1
Remanent flux density of the magnets	B_{rm}	1.1 T at 85 °C
Iron loss per unit mass	P_{Fe0}	4.9 W/kg at 50 Hz and 1.5 T
Copper resistivity	ρ_{Cu}	0.0252 μΩm at 120 °C
Copper fill factor	k_{sfil}	0.6
Number of conductors per slot	N_s	6
Number of slots per pole per phase	N_p	1

to tackle nonlinear effects occurring in the hydrodynamic stage of WECs. Hence, only a brief overview of the derivation of the equivalent linear coefficients is provided here, and more details of the derivation can be referred to Roberts and Spanos (2003). For a nonlinear function F_{non}, expressed as

$$F_{non} = f(v) \tag{B.1}$$

where v stands for a zero-mean random variable and $f(v)$ represents mathematic formula with respect to v. Let its linear approximation function, denoted as $f_{eq}(v)$, be expressed as

$$f_{eq}(v) = Nu + Q \tag{B.2}$$

here, N embodies the equivalent linearized representations, which can be $R_{vis,eq}$ or $R_{pto,eq}$ in (27); Q is the mean part of the nonlinear function f_v. The error introduced by the linearization is then calculated as

$$\epsilon = f(v) - Nu - Q \tag{B.3}$$

For a stochastic process, the expected value of the error squared, namely $\mathbf{E}\left[\epsilon^2\right]$, can be derived as

$$\mathbf{E}\left(\epsilon^2\right) = \mathbf{E}\left[(f(v) - Nu - Q)^2\right] \tag{B.4}$$

where $\mathbf{E}(\cdot)$ represents the expected value of a function. Minimizing the squared error requires N and Q to satisfy the following conditions:

$$\frac{\mathrm{d}}{\mathrm{d}N}\mathbf{E}\left(\epsilon^2\right) = 0 \quad \text{and} \quad \frac{\mathrm{d}}{\mathrm{d}Q}\mathbf{E}\left(\epsilon^2\right) = 0 \tag{B.5}$$

This leads to

$$N = \frac{\mathbf{E}\left[vf(v)\right]}{\mathbf{E}\left(u^2\right)} = \frac{\mathbf{E}\left[vf(v)\right]}{\sigma_v^2} \tag{B.6}$$

$$Q = \mathbf{E}\left[f(v)\right] \tag{B.7}$$

where the expected value at the numerator of the equation can be calculated as

$$\mathbf{E}\left[vf(v)\right] = \int_{-\infty}^{\infty} vf(v)p(v)\mathrm{d}v \tag{B.8}$$

where σ_v is the standard deviation of the variable v; $p(v)$ is the probability density function of the variable v. Assuming that the variable v follows Gaussian distribution, the probability density function is then expressed as

$$p(v) = \frac{1}{\sigma_v\sqrt{2\pi}}\exp(-\frac{v^2}{2\sigma_v^2}) \tag{B.9}$$

Substituting (B.9) into (B.8) yields the equivalent coefficients.

Regarding the viscous drag effect and the PTO force saturation considered in this work, their mean values are equal to zero when substituting (5) and (6) into (B.7). The corresponding linearized equivalent coefficients, $R_{vis,eq}$ and $R_{pto,eq}$, are derived by substituting (5) and (6) into (B.6). Further details of the derivation procedure for these particular two nonlinear effects can be found in Tan et al. (2022a).

References

Albert, A., Berselli, G., Bruzzone, L., Fanghella, P., 2017. Mechanical design and simulation of an onshore four-bar wave energy converter. Renew. Energy 114, 766–774.

Avalos, G.O.G., Peña, J.C.U., Rodríguez, C.L.M., 2024. Preliminary study of the performance of a new wave energy converter. J. Ocean. Eng. Mar. Energy 10 (1), 125–136.

Avalos, G.O.G., Shadman, M., Estefen, S.F., 2021. Application of the latching control system on the power performance of a wave energy converter characterized by gearbox, flywheel, and electrical generator. J. Mar. Sci. Appl. 20 (4), 767–786.

Blanco, M., Villalba, I., Lafoz, M., Nájera, J., Navarro, G., Santos-Herrán, M., 2025. Power optimization modelling as a computational tool for power take off design in wave energy converters. Appl. Ocean Res. 160, 104628.

Bosma, B., Zhang, Z., Brekken, T.K., Özkan-Haller, H.T., McNatt, C., Yim, S.C., 2012. Wave energy converter modeling in the frequency domain: A design guide. In: 2012 IEEE Energy Conversion Congress and Exposition. ECCE, IEEE, pp. 2099–2106.

Coe, R.G., Bacelli, G., 2023. Useful power maximization for wave energy converters.

Cummins, W., Iiuhl, W., Uinm, A., 1962. The impulse response function and ship motions.

da Silva, L.S., Cazzolato, B.S., Sergiienko, N.Y., Ding, B., Morishita, H.M., Pesce, C.P., 2020. Statistical linearization of the morison's equation applied to wave energy converters. J. Ocean. Eng. Mar. Energy 6 (2), 157–169.

Dang, T.D., Phan, C.B., Ahn, K.K., 2019. Modeling and experimental investigation on performance of a wave energy converter with mechanical power take-off. Int. J. Precis. Eng. Manuf.-Green Technol. 6 (4), 751–768.

De O. Falcão, A., Rodrigues, R., 2002. Stochastic modelling of OWC wave power plant performance. Appl. Ocean Res. 24 (2), 59–71.

Drew, B., Plummer, A.R., Sahinkaya, M.N., 2009. A review of wave energy converter technology. Proc. Inst. Mech. Eng. A 223 (8), 887–902.

Ermakov, A.M., Rose-Butcher, J.L., Ringwood, J.V., 2024. On the value of Fano resonance in wave energy converters. Appl. Ocean Res. 153, 104276.

Falnes, J., 2003. Ocean waves and Oscillating systems. vol. 30, p. 953, 7.

Folley, M. (Ed.), 2016. Numerical Modelling of Wave Energy Converters.

Folley, M., Whittaker, T., 2010. Spectral modelling of wave energy converters. Coast. Eng. 57 (10), 892–897.

Folley, M., Whittaker, T., 2013. Validating a spectral-domain model of an OWC using physical model data. Int. J. Mar. Energy 2, 1–11.

Gunawardane, S., Folley, M., Sanjaya, S., 2017. Spectral-domain modelling of the non-linear hydrostatic stiffness of a heaving-sphere wave energy converter. In: Proceedings of the 28th International Symposium on Transport Phenomena, Peradeniya, Sri Lanka. pp. 22–24.

Hals, J., Falnes, J., Moan, T., 2010. Constrained optimal control of a heaving buoy wave-energy converter. J. Offshore Mech. Arct. Eng. 133 (1), 011401.

Journée, J.M.J., Massie, W.W., Huijsmans, R.H.M., 2015. Offshore hydrodynamics.

Liang, C., Ai, J., Zuo, L., 2017. Design, fabrication, simulation and testing of an ocean wave energy converter with mechanical motion rectifier. Ocean Eng. 136, 190–200.
Penalba, M., Cortajarena, J.-A., Ringwood, J.V., 2017a. Validating a wave-to-wire model for a wave energy converter—Part II: The electrical system. Energies 10 (7), 1002.
Penalba, M., Kelly, T., Ringwood, J., 2017b. Using NEMOH for modelling wave energy converters: A comparative study with WAMIT. In: 12th European Wave and Tidal Energy Conference. p. 10.
Penalba, M., Ringwood, J.V., 2016. A review of wave-to-wire models for wave energy converters. Energies 9 (7).
Penalba, M., Ringwood, J.V., 2019. A high-fidelity wave-to-wire model for wave energy converters. Renew. Energy 134, 367–378.
Penalba, M., Sell, N.P., Hillis, A.J., Ringwood, J.V., 2017c. Validating a wave-to-wire model for a wave energy converter—Part I: The hydraulic transmission system. Energies 10 (7), 977.
Pennock, S., Dickson, M., Rebenius, K., Todalshaug, J.H., 2025. Results and lessons learned from CorPower ocean's full scale C4 wave energy converter first ocean deployment period. In: Proceedings of the European Wave and Tidal Energy Conference. vol. 16.
Pérez, T., Fossen, T., 2008. Time-vs. frequency-domain identification of parametric radiation force models for marine structures at zero speed. Model. Identif. Control 29 (1), 1–19.
Polinder, H., Damen, M.E.C., Gardner, F., 2004. Linear PM generator system for wave energy conversion in the AWS. IEEE Trans. Energy Convers. 19 (3), 583–589.
Polinder, H., Van der Pijl, F.F., De Vilder, G.-J., Tavner, P.J., 2006. Comparison of direct-drive and geared generator concepts for wind turbines. IEEE Trans. Energy Convers. 21 (3), 725–733.
Ringwood, J.V., 2025. Control co-design for wave energy systems. Appl. Ocean Res. 158, 104514.
Roberts, J.B., Spanos, P.D., 2003. Random Vibration and Statistical Linearization. Courier Corporation.
Shadman, M., Avalos, G.O.G., Estefen, S.F., 2021. On the power performance of a wave energy converter with a direct mechanical drive power take-off system controlled by latching. Renew. Energy 169, 157–177.
Silva, L.S.P.d., 2019. Nonlinear Stochastic Analysis of Wave Energy Converters Via Statistical Linearization (Ph.D. thesis). Universidade de São Paulo.
Silva, L., Sergiienko, N., Pesce, C., Ding, B., Cazzolato, B., Morishita, H., 2020. Stochastic analysis of nonlinear wave energy converters via statistical linearization. Appl. Ocean Res. 95, 102023.
Son, D., Yeung, R.W., 2017. Real-time implementation and validation of optimal damping control for a permanent-magnet linear generator in wave energy extraction. Appl. Energy 208, 571–579.
Spanos, P.D., Strati, F.M., Malara, G., Arena, F., 2018. An approach for non-linear stochastic analysis of U-shaped OWC wave energy converters. Probab. Eng. Mech. 54, 44–52.
Tan, J., Coe, R.G., Lavidas, G., 2025a. Benchmark of numerical modeling approaches on the systematic performance evaluation of wave energy converters. Appl. Ocean Res. 162, 104725.
Tan, J., Laguna, A.J., 2023. Spectral-domain modelling of wave energy converters as an efficient tool for adjustment of PTO model parameters. In: Proceedings of the European Wave and Tidal Energy Conference. vol. 15.
Tan, J., Lavidas, G., 2024. A modified spectral-domain model for nonlinear hydrostatic restoring force of heaving wave energy converters. Ocean Eng. 309, 118581.
Tan, J., Polinder, H., Laguna, A.J., Miedema, S., 2022a. The application of the spectral domain modeling to the power take-off sizing of heaving wave energy converters. Appl. Ocean Res. 122, 103110.
Tan, J., Polinder, H., Wellens, P., Miedema, S., 2020. A feasibility study on downsizing of power take off system of wave energy converters. In: Developments in Renewable Energies Offshore. CRC Press, pp. 140–148.
Tan, J., Wang, X., Jarquin Laguna, A., Polinder, H., Miedema, S., 2021. The influence of linear permanent magnet generator sizing on the techno-economic performance of a wave energy converter. In: 2021 13th International Symposium on Linear Drives for Industry Applications. LDIA, pp. 1–6.
Tan, J., Wang, X., Polinder, H., Laguna, A.J., Miedema, S.A., 2022b. Downsizing the linear PM generator in wave energy conversion for improved economic feasibility. J. Mar. Sci. Eng. 10 (9), 1316.
Tan, J., Xi, C., Lavidas, G., Zhou, B., 2026. Computationally-efficient wave-to-wire modeling of wave energy converter arrays based on a spectral-domain approach. Ocean Eng. 347, 123942.
Tan, J., Zuo, L., Lavidas, G., Metrikine, A., 2025b. Extending the statistical linearization method to multi-variate non-differentiable nonlinearities in floating renewable energy devices. Renew. Energy 123964.
Yi, Y., Sun, K., Liu, Y., Zhang, J., Zhang, H., Zhu, R., Yao, H.-D., 2026. Coupled numerical framework for wind-wave-to-wire energy conversion in floating hybrid wind-wave systems. Appl. Energy 403, 127106.